Fire Safety Journal 114 (2020) 103009

Contents lists available at ScienceDirect

Fire Safety Journal

journal homepage: http://www.elsevier.com/locate/firesaf

Early detection of smoldering in silos: Organic material emissions as precursors

Nir Bluvshtein [a,c], Edmundo Villacorta [b], Chunlin Li [a], Bjarne C. Hagen [b,*], Vidar Frette [b], Yinon Rudich [a]

[a] Department of Earth and Planetary Sciences, Weizmann Institute of Science, Rehovot, 76100 Israel
[b] Western Norway University of Applied Sciences, Bjørnsonsgt. 45, N-5528, Haugesund, Norway
[c] Currently at Institute for Atmospheric and Climate Science, ETH Zürich, 8092, Zürich, Switzerland

A B S T R A C T

The possible use of organic particle emissions as indicators of smoldering fires at low temperatures (early stages, <150 °C) is explored in laboratory experiments. Samples consisting of wood pellets were heated under controlled atmosphere. The sample temperature was slowly ramped, mimicking the spontaneous, slow temperature increase during self-heating in organic materials. As the sample temperature reached 90–100 °C, a two-orders-of-magnitude increase in the number concentration of sub-micrometer particulate matter was measured under both air and nitrogen atmosphere. A detailed analysis of their chemical composition indicated that the particles formed through evaporation of low-volatile organic compounds followed by condensation downstream of the heated volume. The increase in aerosol concentration precedes any significant increase in measured CO and CO_2 concentration in both time and temperature. Our results suggest that the sub-micron particle concentration could be considered as an indication of the stages that lead to smoldering fires.

1. Introduction

Early detection of smoldering fires in combustible, granular organic materials is crucial to prevent escalation, transition to flaming fire, and explosions. If not detected at an early stage, smoldering fire in large-volume storing facilities may escalate to a point where little can be done to control or extinguish the fire. As the stored material and silo structure are destroyed by the fire, harmful particulate material and gasses are emitted to the atmosphere, and economic losses and environmental damage are inevitable [1].

Materials in granular form such as grains and other foods, animal and fish feed and biomass fuels are commonly stored in silos in large quantities. Wood-based fuels are of particular concern. With increasing demand for commercial fuels for residential heating and energy production, along with depletion of fossil fuel resources and introduction of emission regulations, biomass represents an important alternative [2].

Wood pellets are the most refined form of wood-based biofuel. It is homogeneous, easily transported and automatically fed to both small- and large-scale combustion units. However, as for many granular materials stored in large quantities, smoldering fires induced by self-heating is a concern [1]. The thermal isolation provided by the large amount of material, as well as the lack of ventilation deep within the pile, facilitates the buildup of heat generated by slow oxidation at moderate temperatures. This heat accelerates the oxidation process by providing a positive feedback through increasing temperatures [3].

Numerous incidents of flaming fires and explosions in storage facilities, caused by escalation of weak smoldering fires, are reported in the literature. Smoldering fires in silos storing wood pellets were reported in Esbjerg, Denmark, (1998–1999) [4] and in Hallingdal, Norway (2010) [5]. In both cases, high CO levels were detected by warning systems during early stages, but did not provide sufficient response time to prevent escalation. A smoldering fire, reported in a grain silo in the USA, started through self-heating caused by the metabolism of molds. In this case, the smoldering transitioned into flaming fire and two explosions occurred due to ignition of CO gas and dust [6]. A silo in Macerate, Italy, storing sawdust and wood chips exploded with fatal results. Frictional heat from a broken screw conveyor started a self-heating process that led to production of flammable gases [7]. In all of the above incidents, the smoldering fire and consequent damage originated from a weak self-heating process. This demonstrates the importance and urgency of early detection of smoldering fires in storage facilities.

Fire detection is currently achieved using various techniques, by tracking changes in temperature, gas emissions and thermal and visible radiation. Smoldering fires have proven difficult to detect due to low heat and smoke production, with low signal-to-noise ratio as a result. To detect smoldering fires, thermocouples are used to monitor temperature

* Corresponding author.
E-mail address: bch@hvl.no (B.C. Hagen).

https://doi.org/10.1016/j.firesaf.2020.103009
Received 5 July 2019; Received in revised form 16 April 2020; Accepted 18 April 2020
Available online 23 April 2020

variations in stored material in silos, which are indicative of increased chemical and thermal processes in the material [4]. When temperature irregularities are detected, steps are taken to empty the silos and cool the stored material. However, it is impractical to cover large-volume silos with temperature sensors to allow for high spatial resolution. Furthermore, temperature sensors necessitate a mechanical structure to be kept in position. Such structures will hinder operations like filling and emptying of silos.

More common detector systems like smoke, flame and gas detectors all have the disadvantage of primarily reacting to already ongoing combustion [8]. Recent detector systems use algorithms such as neural networks [9] and e-noses [10] to detect fires. These systems can also incorporate detections of specific gases or compounds to enhance the detection accuracy and to decrease warning time. One example is levoglucosan, which was recently reported as a tracer in particulate matter emitted during smoldering fires [11]. In the future, increased use is expected of systems that integrate detectors of several types and employ advanced algorithms to interpret their signals. A relevant example can be found in Ref. [9]. Here, a commercial machine-learning algorithm is used to discriminate between smoke from a series of different fuels. Currently, still, all systems suffer from the same inherent disadvantage. They all use signals based on smoke, flames and gases from combustion that is already ongoing.

Thus, it may be beneficial to base detection on the processes that precede pyrolysis and combustion as temperature increases – commonly referred to as preheating and drying [12,13]. Although these terms may leave the impression that during these stages, merely evaporation of water occurs, the underlying processes, beyond water evaporation, are complex and not well understood.

Studies focused on air quality and air pollution emissions from wood drying processes reported increased emission of volatile organic compounds, and low-volatility organic compounds (VOCs and LVOCs) at temperature range 100–200 °C. The compounds emitted are primarily monoterpenes but could also include fatty acids, resin acids, diterpenes and triterpenes. At the upper end of this temperature range, thermal degradation products of VOCs and LVOCs were also detected [14].

In this study, we investigate sub-micrometer (accumulation mode) organic particulate matter emitted at characteristic elevated temperature (90–140 °C). We hypothesize that some of the VOCs and LVOCs emitted in this temperature range form sub-micrometer particles through nucleation, growth and coagulation upon cooling to room temperature. Furthermore, due to the relatively low temperature, we expect negligible emissions of high-volatility gasses such as CO and CO_2 from pyrolysis.

2. Experimental set-ups and procedures

To simulate pre-heating and drying of wood pellets, we have used a tube-shaped oven that allows slow and spatially homogeneous temperature increase of samples. The tube oven consists of a 60 × 10 × 10 cm aluminum block (length · width · height) surrounding a 70 cm long, 2.54 cm in diameter stainless steel tube serving as the fuel compartment (Fig. 1). A 600 W heating element, 13 mm in diameter (red line in Fig. 1), and a temperature controller (2216L, Eurotherm) was used to regulate the temperature of the fuel compartment with accuracy 0.1 °C. The tube oven was cooled by convection from its outer surface. 100 g of wood pellets (Table 1) was inserted into the fuel compartment and the temperature ramped from room temperature to 135 °C in 20, 10 or 5 °C steps. At each step, the new temperature was held constant for 15–60 min to observe changes in both aerosol and gaseous emissions. Purified air or N_2 at 0.3 L/min was introduced into the fuel compartment via a copper tube (inner diameter 6.5 mm) pre-heated to the tube oven temperature. Due to the low moisture content (<10%, Table 1) in the wood pellets, the sample temperature is assumed here to match the oven temperature. The gas/aerosol outflow from the oven was cooled by a double-jacket glass condenser with continuous circulation of water at 5 °C through its external jacket. Condensed liquid accumulated in a vial at the bottom of the condenser and was thus separated from the outflow. Additional dehydration (RH < 15%) and equilibration to room temperature (T ≈ 20 °C) was achieved through dilution of the outflow by a factor of about 7 using 1.7 L/min purified air or N_2. Purified air was supplied by a compressed-air treatment system (BSP-MT1; Parker Zander) that removed humidity, CO_2, particulate and gaseous pollutants from ambient compressed (8 bar) air.

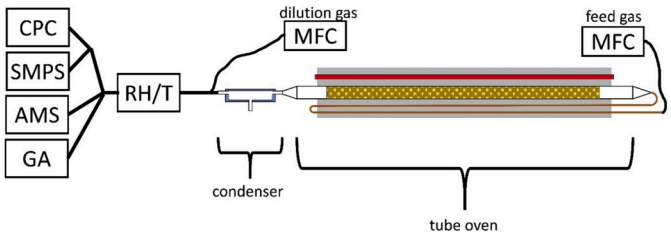

Fig. 1. Schematic description of the tube oven setup. MFC; mass flow controller. RH/T; relative humidity and temperature sensor. CPC; condensation particle counter. SMPS; scanning mobility particle sizer. AMS; aerosol mass spectrometer. GA; gas analyzers.

Table 1
Material properties of the wood pellets (produced by Hallingdal trepellets, ÅI, Norway), with methods used.

Material properties	Wood Pellets
Type of material	Wood (including bark) 20–50% pine 50–80% spruce
Pellet diameter [mm]	8
Unit density [kg/m^3]	1020
Bulk density [kg/m^3]	710
Porosity [%]	30.4
Moisture content [%]*[a]	**6.3** (6.8)
Volatile compounds [%]*[b]	**77** (82)
Ash content [%]*[b]	**0.46** (0.49)
Elemental composition [%]*[c]	
Carbon (C)	**48** (48) *[52]*
Hydrogen (H)	**6** (6) [6]
Nitrogen (N)	**0** (0) *[0]*
Oxygen (O) & Others	**39** (39) *[42]*

*) Denoted as: **Ambient conditions** (Air dried) *[Water and ash free]*.
a) Determined using Thermogravimetric Analyzer and Moisture Analyzer.
b) Determined using Thermogravimetric Analyzer. Defined as the amount of the material which undergoes pyrolysis and primary oxidation to form char.
c) Determined using Thermogravimetric Analyzer and Carbon/Hydrogen/Nitrogen Determinator.

The tube oven, with the flow arrangements described above, has the following characteristics, which are crucial to obtain the results reported below: Homogeneous sample heating, with reliable temperature control at moderate temperatures (preheated carrier gas), strict control of the composition, temperature, and humidity of carrier gas, with carrier gas free of particles, CO_2, and CO upon entering the sample. Note in particular that due to the air flow through the sample, the detected emissions truly reflect the current state of the sample, and not (in part) previous states.

After leaving the RH/T units, the combined aerosol flow was split iso-kinetically to the monitoring instruments. A condensation particle counter (CPC; 3022A, TSI) measured total particle number concentration (counting efficiency > 95% for particle diameter > 20 nm), while a scanning mobility particle sizer (SMPS, TSI; consists of 3080 Classifier, 3081 DMA, and a 3775 CPC) measured the size distribution of the fine-mode (0.015–0.7 μm) polydisperse particles that were either directly emitted or formed in the process. Two gas analyzers (GA) were used to record CO, O_2 (PLT-400, Eranntex) and CO_2 concentration (GasHound Li-800, LI-COR) of the outflow.

On-line chemical characterization of the particles was obtained using an Aerodyne high-resolution time-of-flight mass spectrometer (HR-ToF-AMS). The AMS provides real-time aerosol mass-spectrometry measurements of the particle-bound organics, sulfate, nitrate, chloride, and ammonium fractions (non-refractory components). The AMS enables identification of markers for biomass burning processes and provides information on carbon oxidation state and types of organic functional groups by quantification of oxygen-to-carbon (O/C) and hydrogen-to-carbon (H/C) elemental ratios. AMS-measured data was analyzed using the SQUIRREL software (v1.12 and PIKA v1) [15].

Supplementary experiments were carried out using an open-top cylinder, similar to the one used in Ref. [16–18], to initiate and study self-sustained smoldering. Fig. 2 shows the variant used in the present case, hereafter referred to as the combustion chamber. Here, 1 kg of wood pellets was placed inside an insulated, 15 cm diameter, 30 cm high, steel tube that rested on an aluminum hotplate. The hotplate was used to simulate self-heating of the wood pellets. The temperature of the hotplate was regulated using two 250 W, 1.27-cm diameter, 10-cm long cylindrical heating elements. The top of the steel tube was left open to allow for convective exchange of gases between the sample and the (un-filtered) laboratory atmosphere. A thermocouple matrix was placed at 2 cm vertical spacing inside the fuel pile along the axis of the steel tube. The combustion chamber was placed on top of a digital scale used to monitor changes in sample mass as the temperature of the hotplate, at the base of the sample, was increased.

Air at a flow rate of 0.23 L/min was pulled from the center of the chamber, with a ¼" stainless steel tube at the top of the fuel pile, about 9 cm above the level of the hotplate. The sample flow was diluted with 2.04 L/min purified air and pulled into the sampling suite, which included measurements of aerosol size distribution (mobility diameter in the range of 0.015–0.7 μm using the SMPS and aerodynamic diameter in the range of 0.6–20 μm using an aerodynamic particle sizer - APS, 3021; TSI) and concentration, in addition to CO, CO_2 and O_2 gas concentration (Fig. 2).

3. Results

Experimental results are described in this section, for nitrogen (Section 3.1) and air (section 3.2) atmosphere. Figs. 3B and 7B below gives our main results: a strong increase in the concentration of particles emitted from the sample, before (at lower temperature) than any significant increases in CO and CO_2 concentrations. We suggest that the reader concentrate first on these two figures and the first paragraph in each of sections 3.1 and 3.2. Some readers may want to move directly from this material to Section 3.3.

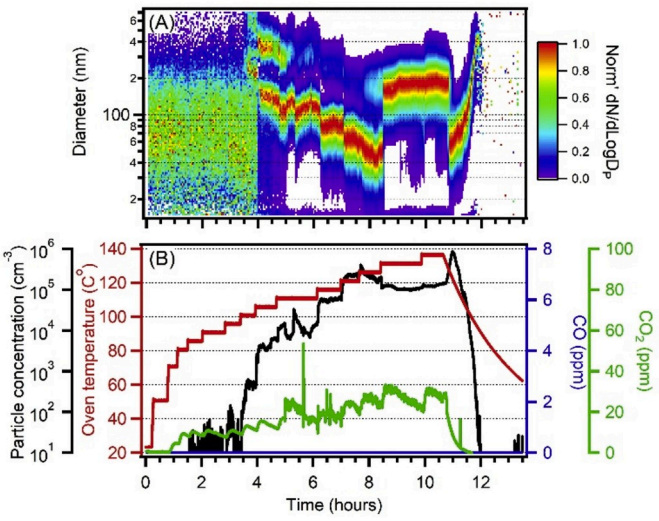

Fig. 3. (A) Size distribution of particles from heating of wood pellets, normalized by the concentration of the mode diameter. (B) Particle number, CO and CO_2 concentrations with changing tube oven temperature, with N_2 as the carrier gas. By definition, the mode diameter is the most frequent diameter value.

The remaining parts of subsections 3.1 and 3.2 discuss the dynamical evolution and the chemical composition of the emitted particles. These more detailed results substantiate the claim that the detected particles originate from the wood pellets sample, and not from any other source.

Section 3.3 discusses additional experiments carried out using the set-up shown in Fig. 2. The conditions the wood pellets sample was exposed to in this case differ from those in the main experiments, and no significant increase in the particle concentration was detected.

3.1. Experiments with N_2 as carrier gas

Fig. 3 shows the evolution of the fine-mode particle size-distribution (normalized by the concentration at the mode diameter) (Fig. 3A), total aerosol number concentration, CO and CO_2 concentration and the tube oven temperature (Fig. 3B) when N_2 was used as the carrier gas. We note

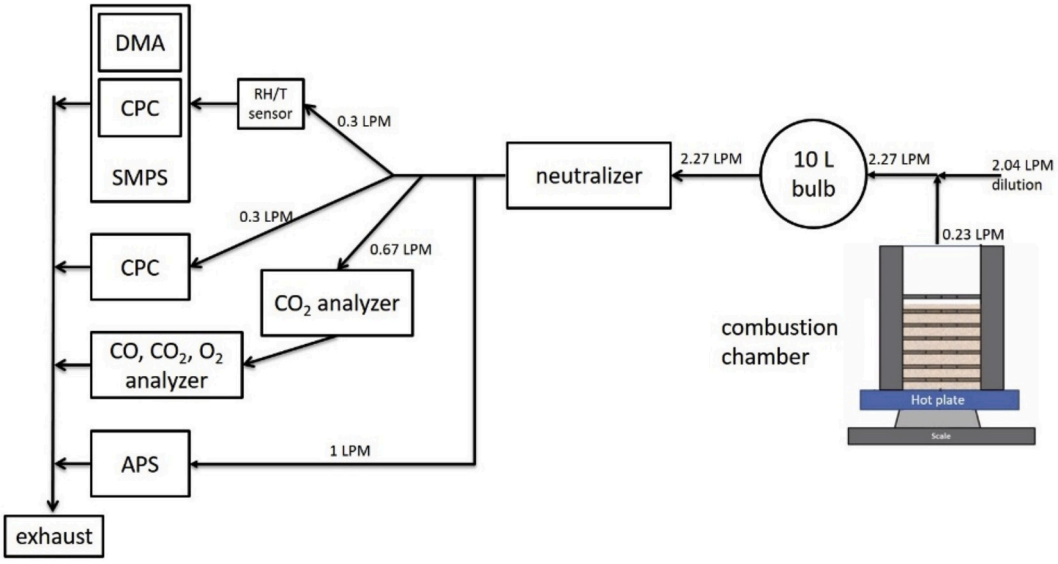

Fig. 2. Schematic description of the sampling set-up and instruments used during the combustion chamber experiment.

here that when the oven temperature (red curve) reached about 100 °C, the concentration of fine-mode particles increased by about two orders of magnitude and continued to increase rapidly up to a temperature of about 125 °C (black curve, logarithmic scale). In contrast to fine-mode particle concentration, CO_2 concentration increased up to about 15 ppm (or 100 ppm in the undiluted sample flow) while CO concentration did not show any measurable increase (detection limit of the sensor is 0.1 ppm, see Fig. 3B). This striking increase in aerosol concentration leads us to propose that a fine-mode particle-concentration signal can be used as an indicator for states that may lead to smoldering combustion.

A more detailed view of the particle-size distribution is given in Fig. 4. This figure shows that the particle size distribution, as the oven temperature is first increased beyond 100 °C and then reduced, exhibits a dual-mode size distribution with modes at about 150 and 350 nm. Interestingly, with increasing temperature (up to about 120 °C) and increasing particle concentration (with a maximum in the range 10^5–10^6 cm^{-3}), the diameter of both modes decreased to about 60 and 160 nm, respectively, and the smaller mode became more dominant (Fig. 3A at 4–8.5 h and Fig. 4A through D). When the temperature increased further (125–135 °C), the particle concentration decreased

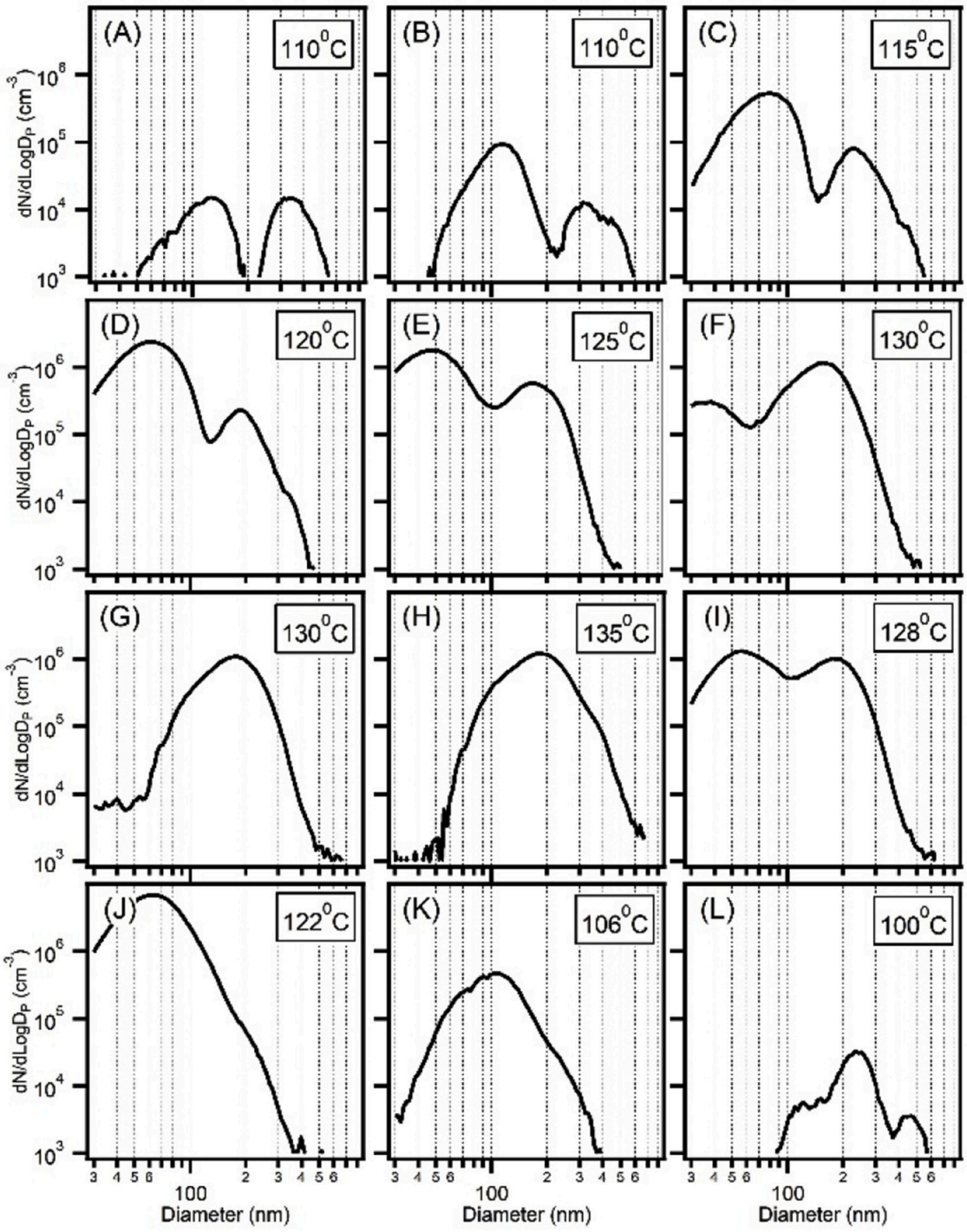

Fig. 4. Evolution of the fine-mode particles size distribution at selected temperatures during the heating and the passive cooling phases for the experiment shown in Fig. 2 with N_2 as the carrier gas.

while the larger mode became more dominant. When the temperature reached 130–135 °C, the smaller mode disappeared completely (Fig. 3A, at around 8.5 h, Fig. 4E through H). When heat was no longer supplied to the oven and passive cooling started, the smaller size mode increased again (Fig. 3A, at around 10.75 h and Fig. 4I to J). This was followed by monotonic increase in particle size with decreasing temperature (Fig. 3A from 11 to 12 h and Fig. 4 K and L). This last stage can be described as the opposite process to the stepwise heating process in which the particle size decreased with increasing temperature.

HR-Tof-AMS chemical characterization of the emitted particles is shown in Fig. 5, with N_2 as carrier gas. The upper red curve shows the oven temperature. Note that only the portion corresponding to oven temperatures from 100 °C to 135 °C in Fig. 3 is covered in Fig. 5.

Seven ion categories were classified from the AMS mass spectrum, ranging from *m/z* (mass-to-charge ratio) 12 to 350, as C_x^+, $C_xH_y^+$, $C_xH_yO^+$, $C_xH_yO_z^+$, $C_xH_yON^+$, $C_xH_yO_zN^+$, and $C_xH_yN^+$ ($x \geq 1$, $y \geq 1$, $z \geq 2$). These ions are the identified fragments that form during evaporation, fragmentation and subsequent ionization of organic compounds in the emitted particles.

The hydrocarbon fragments ($C_xH_y^+$) dominated the emissions (80.7 wt% on average, in green in Fig. 5C). Notwithstanding, Fig. 5 also shows that the contribution of hydrocarbon fragments decreased slightly with increasing oven temperature, while the contribution of more oxidized fragments increased. This can be more clearly observed in the elemental ratios of oxygen to carbon (O/C) and hydrogen to carbon (H/C), which indicate the oxidation state of the aerosols. While the H/C ratio decreased slightly with increased tube oven temperature, the O/C ratio increased.

The normalized AMS chemical composition of the particles emitted during the experiment (data not shown) contains the prominent fragment ions of hydrocarbons such as $C_nH_{2n-1}^+$ (m/z-values 27, 41, 55, 69 etc.) and $C_nH_{2n+1}^+$ (m/z-values 29, 43, 57, 71 etc.), which are attributed to low-volatile organic compounds (LVOC) [19,20].

The fragment m/z = 43 ($C_2H_3O^+$, characteristic fragment of carbonyl) is commonly considered to be a tracer for fresh organic aerosols. During organic aerosol aging in the ambient environment or in laboratory experiments, fragment m/z = 43 (or the ratio of fragment 43 to the total organics, *f*43) generally decreases with increasing oxidation, while fragment m/z = 44 (CO_2^+, typical carboxyl or organo-peroxide ion) increases [21,22].

Thus, the relationship between the two fragments can provide information about the oxidation level of the analyzed particles, as described in Fig. 6, which demonstrates a positive linear correlation between fragment 43 and 44. This was observed in terms of both mass concentration and mass fraction, indicating enhanced primary emissions of carbonyl and carboxyl functional groups containing carbonaceous aerosol during early-stage heating. The ratio of fragment 44 to fragment 43 was approximately conserved (between 1:2 and 1:1.5) throughout the experiment and was not clearly dependent on the oven temperature, which means that the two fragments were co-emitted and do not result from an oxidative combustion process.

3.2. Experiments with air as carrier gas

When purified air is used as the carrier gas, the fine mode particle size distribution and concentration changed with increasing temperature similarly to when N_2 was used as the carrier gas (Fig. 7), although at the slightly lower temperature of 90 °C. The CO_2 concentration gradually increased with temperature up to about 110 °C. At higher temperatures, both CO_2 and CO increased, with CO_2 peaking at over 95 ppm (≈640 ppm in the undiluted sample flow) and CO peaking at 7 ppm (≈50 ppm in the undiluted sample flow) at 135 °C. The variations in the particle size distribution with temperature (data not shown) were similar to the case with nitrogen atmosphere (Fig. 4).

No significant differences were observed in the particles' chemical composition measured with the AMS when air was used as the carrier gas (data not shown) but as expected, with available oxygen, the oxidation level of the measured particles was slightly higher. Hydrocarbon fragments were still the major components of the detected aerosols (around 79 wt%). The trends in O/C and H/C ratios with

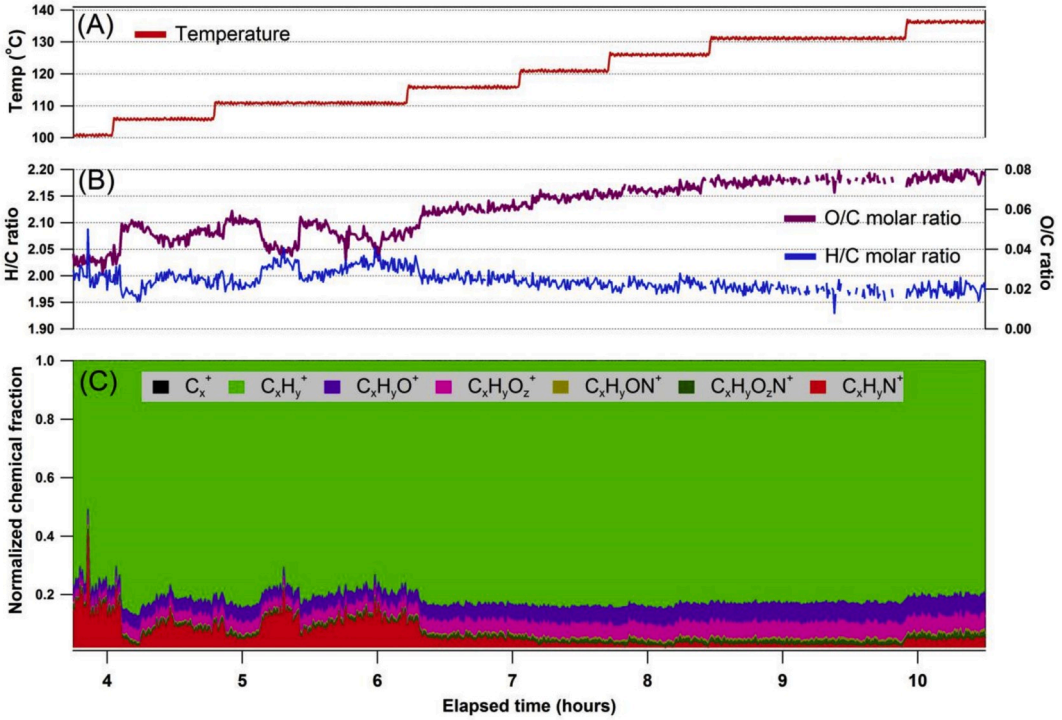

Fig. 5. Evolution in chemical characteristics of wood pellet particulate emissions from stepwise low-temperature heating with N_2 as carrier gas. (A) Oven temperature, (B) elemental ratios from bulk chemical HR-Tof-AMS results, (C) detailed chemical fragment composition with seven ion groups, which were classified based on the mass spectrum analysis as C_x^+, $C_xH_y^+$, $C_xH_yO^+$, $C_xH_yO_z^+$, $C_xH_yON^+$, $C_xH_yO_zN^+$, $C_xH_yN^+$ ($x \geq 1$, $y \geq 1$, $z \geq 2$).

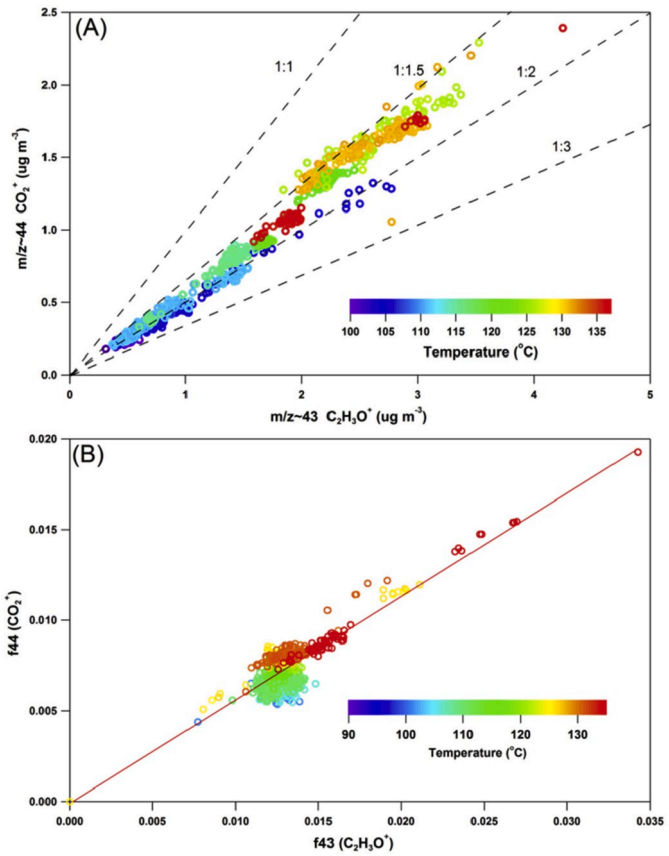

Fig. 6. Regression analysis of fragments at m/z = 43 and 44 from organic aerosols released during the experiment with N_2 as carrier gas. Regression of the m/z 44 and 43 fragments as mass concentration (A) and as fraction of total mass (B).

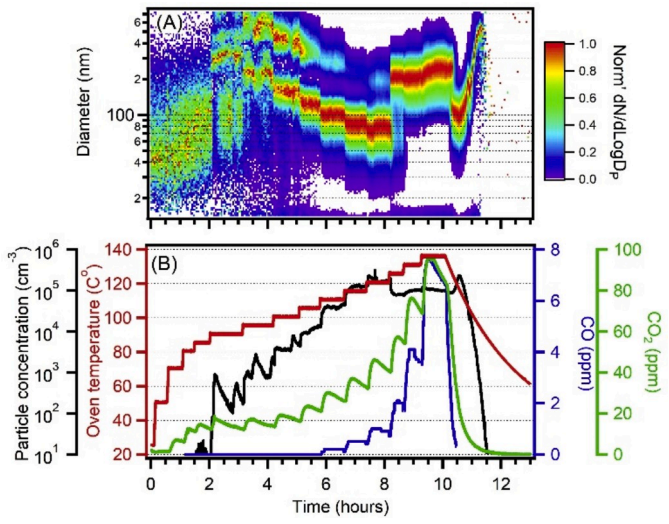

Fig. 7. Size distribution of particles from heating of wood pellets, normalized by the concentration of the mode diameter (A). Particle, CO and CO_2 concentrations and oven temperature with air as the carrier gas (B).

increasing oven temperature were similar to when N_2 was the carrier gas.

Unlike in section 3.1, where N_2 was used as the carrier gas, regression analysis of the fragments m/z 44 and 43 showed some temperature dependence. The ratio of fragment 44 to fragment 43 is higher at elevated temperature (Fig. 8A). This temperature dependence can also be observed in the negative correlation between mass fraction *f*44 and *f*43 (Fig. 8B).

3.3. Non-homogeneous sample temperature

Fig. 9 shows the temperature of the hotplate and of the fuel pile environment at several heights above the hotplate for a typical experiment using the setup in Fig. 2. The upper, step-shaped curve shows the temperature imposed at the bottom of the sample, while the other curves show temperatures measured at various levels inside and above the sample. At any point in time, the temperature decreases systematically as one moves away from the heat source.

The temperature curve suggests that the wood pellets at the bottom layer of the pile (up to a height of about 1–2 cm) should have experienced the same conditions as in the tube oven experiment. Additionally, the mass lost during the experiment (>8%) is higher than the reported moisture content in the wood pellets (<7%, Table 1). This suggests that at least some of the lost mass is indeed organic material. It is therefore reasonable to assume that the same processes would take place, i.e. formation of particles by evaporation and condensation. However, no significant increase in particle concentration was detected.

There were also visible differences between the various layers of the sample following heating and between the two types of experiments. The wood pellets from the bottom of the fuel pile, which was exposed to temperatures as high as 200 °C, showed a distinct change in color (darker brown, typical before charring) (Fig. 10) while the pellets from the tube oven experiments showed none. Furthermore, the concentration of CO, CO_2, and particles did not increase above background levels

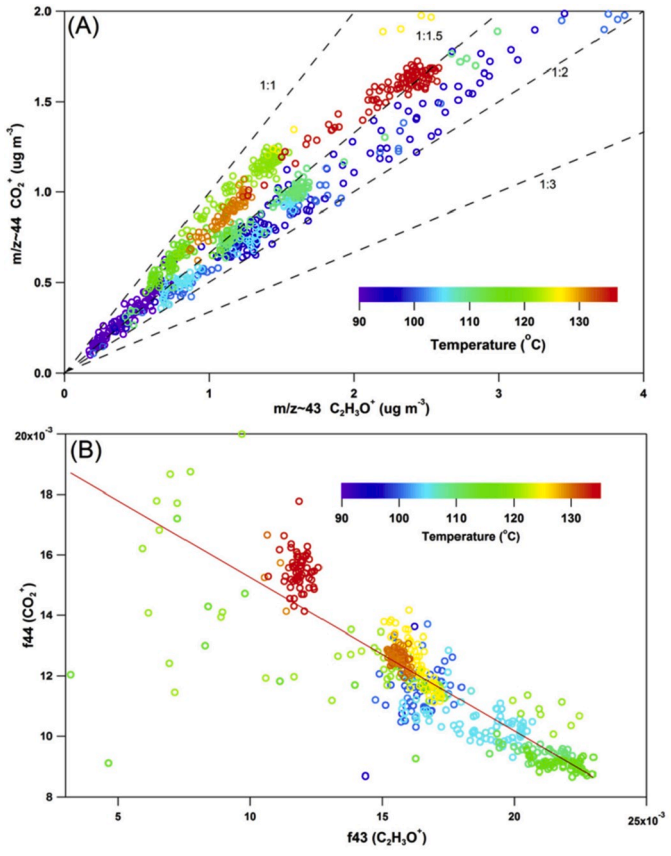

Fig. 8. Regression analysis of fragments at m/z = 43 and 44 from organic aerosols (particles) released during the experiment (O_2 as carrier gas). Regression of the m/z 44 and 43 fragments as mass concentration (A) and as fraction of total mass (B).

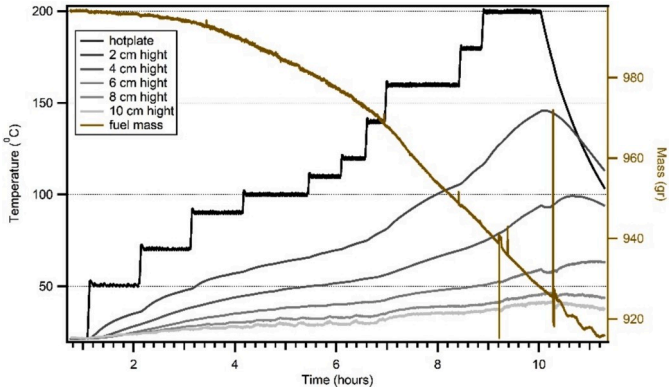

Fig. 9. Temperature of the hotplate and at several heights in the 9 cm high wood pellets pile, as functions of time. The (decreasing) sample mass is also shown.

(data not shown). Measured CO_2-levels varied within a 10 ppm range, which correlates to a 100 ppm range of the undiluted sampled flow. This variation is attributed to variation in background room CO_2 levels due to presence of people in the laboratory.

4. Discussion

As the temperature of wood pellets samples gradually increased, a strong particle emission was detected at about 100 °C. This is the typical temperature range where drying occurs in a process leading to ignition of smoldering [12]. At this stage, VOCs and LVOCs are released from the solid phase [23]. Downstream from the emission source, where the temperature drops back to ambient conditions, some of the organic compounds condense and coagulate to form fine-mode particles, explaining the particle changes detected as described above [24]. The strong increase in the particle concentration occurred both under N_2 and air atmosphere, two situations that represent oxygen-depleted regions deep in a storage silo – and oxygen-rich regions close to its top level, respectively. This process precedes CO and CO_2 release.

The interplay between the two size modes described in section 3.1 and in Fig. 4 (and also found for air atmosphere) is probably a result of a complex dynamic competition between nucleation and growth; the two physical processes controlling new particle formation. While growth depends on the physico-chemical properties of the emitted gaseous species and the surface available for condensation, nucleation is mostly concentration (and thereby, temperature) limited. It is also conceivable that above 120 °C, partial thermal degradation of LVOCs takes place, reducing their concentration thereby suppressing nucleation. This could explain the decrease in total particle concentration above this temperature (Figs. 3 and 7) as well as the disappearance of the small-size mode. This hypothesis is not further discussed in this work as a detailed analysis of particle formation processes is beyond the scope of this study.

The small increase in CO_2 concentration at low temperature above room temperature (50–80 °C) shown in Figs. 3 and 7 may be related to release of gas that is trapped within the porous medium following microbial activity during storage. We believe that this increase would be within natural variability of elevated background levels in a high-load storage facility. Furthermore, Figs. 3 and 7 show that the increase in particle concentration is significantly stronger than the increases in CO and CO_2. While the particle concentration increases by two orders of magnitude, the CO concentration did not increase at all when N_2 was used as the carrier gas. When air was used and oxygen was available, the CO concentration increased above background level but at a higher temperature than the increase in particle concentration. Some devices designed to detect smoldering fires are based on measurement of the CO concentration. Our results indicate, however, that CO did not form at detectable levels below 110 °C and under oxygen-depleted atmosphere conditions. Interestingly, in Ref. [25] the main increase in CO concentration also occurs from temperatures around 110 °C on (see their Fig. 2). However, a detailed comparison with our results is precluded, due to differences in heating and sampling protocols. No measurements on particle concentrations were carried out in the cited paper.

At oven temperatures above the aerosol generation threshold (>100 °C) VOCs and LVOCs such as carboxylic acids, could be an additional source for gas-phase CO_2 via thermal decomposition.

As for costs, equipment for measurements of sub-micrometer particles is currently expensive compared with CO and CO_2 detectors. However, there are new generations of low-cost sensors (such as Alphasense N3 – about $250) that are emerging and can be added to the detection system at low costs. On the other hand, its detection range starts at particles with diameters 350 nm, which is somewhat large for our situation.

It is important to note that the strong increase in the particle concentration arises from processes that precede smoldering (evaporation

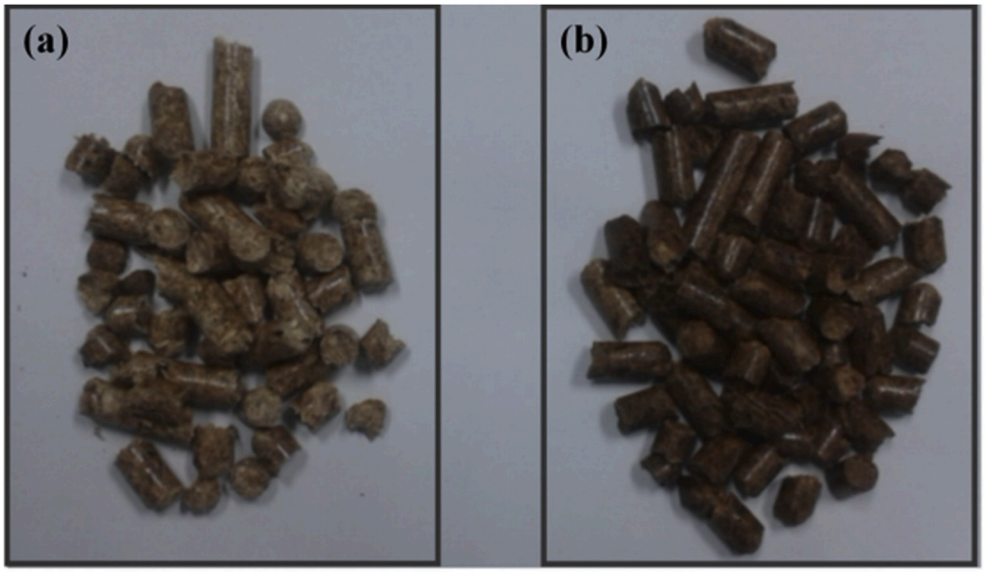

Fig. 10. Wood pellets from the combustion chamber experiment. a) pellets from higher level (not distinguishable from fresh, un-heated fuel), b) Pellets from the bottom layer.

of VOCs and LVOCs, followed by condensation and coagulation) but inevitably will lead to smoldering if the stored material is left undisturbed. Self-heating will result in a slow temperature increase both in a core region and in its surroundings, which in turn intensifies the self-heating processes, until pyrolysis and smoldering occur.

Furthermore, our results suggest that the existence of detectable CO levels depend on the presence of oxygen at ambient concentration. Preferably, this should be avoided in storage silos in order to reduce the risk of ignition.

The analysis of the HR-ToF-AMS measurements conducted during the tube oven experiment (Fig. 5) showed that, unlike for the typical composition of biomass burning aerosols measured in the ambient atmosphere [26,27], inorganic species (e.g., SO_4^{2-}, NO_3^-, Cl^-, NH_4^+) were not detected. This implies that pyrolysis or combustion was not among the processes that caused particle emission during low-temperature heating of the wood pellets. Additionally, the abundance of hydrocarbon fragments ($C_xH_y^+$) (80.7 wt% on average, green area in Fig. 5) points to the hydrocarbon-like, low volatility and low oxidation-state nature of the sampled organic aerosols. The hydrocarbon-like chemical feature implies that these particles mainly formed through condensation of low-volatility organics that evaporated during pre-heating and drying of the wood pellets. The slight increase in more oxidized fragments described by the H/C and O/C molar ratios could be related to release of more oxidized LVOCs at higher temperatures.

The MS spectra described above are significantly different from reported data of standard combustion processes, in which the *m/z* 44 (CO_2^+, characteristic fragment of carboxyl or peroxide) peak has been identified as a marker for oxygenated organic aerosols [28]. This fragment was reported to have a significant contribution of 5–30 wt% in both flaming and smoldering aerosol mass spectra, depending on burning conditions and biofuel type [29]. In the present experiments, however, the CO_2^+ fragment contributed less than 0.5 wt% of the total organics, with maximal contribution of gaseous CO_2 to the m/z 44 signal less than 0.05% [21].

The positive linear correlation between fragments 43 and 44 and its independence on temperature, shown in Fig. 6, indicates that these two fragments are primarily co-emitted, and that the measured particles are not a result of severe oxidation of the solid fuel or of the primary organic material that is directly emitted from the heated wood pellets.

This increase in CO during the tube-oven experiment under purified air atmosphere, starting at about 110 °C, well below the temperature required for initiation of forced pyrolysis (200 °C suggested by García-Perez [30]) indicates that the source of CO_2 up to that point is similar to the case with N_2 as carrier gas. It also implies that the additional contribution to both gases is gas-phase oxidation of released organics, which is made possible with available oxygen, and catalyzed by the elevated temperature.

The temperature dependence and the negative correlation between fragments 43 and 44 with available oxygen (Fig. 8), suggests that *f*44 is a result of aging or oxidation of the primarily emitted gas-phase organic material.

Similarly to when N_2 was used as the carrier gas, there is a lack of inorganic ions and low levels of oxygenated organic ions (data not shown) that implies that the higher O/C ratio is due to release of more oxidized LVOCs at higher temperatures and not due to pyrolysis of the fuel material. With available oxygen, partial gas-phase oxidation of evaporated compounds is also possible.

In contrast to the tube oven experiments, the supplementary combustion chamber test showed no increase in sub-micrometer particle concentration. This difference between the two types of experiments is probably related to the difference in the way the samples were heated. In the tube oven experiments (Fig. 1) the fuel was homogeneously heated, while in the combustion chamber experiment (Fig. 2) only the bottom-most fuel layer was heated, as evident from the temperature profiles in Fig. 9. With non-uniform heating, as expected in large solid fuel deposits, such as pellets silos, the cold pellets provide a large surface for condensation of gaseous LVOC and for wall loss of LVOC-containing particles. As a result, the concentration of particles may be reduced to an extent that no particle signal can be detected outside the sample, as we observed. Furthermore, with wood pellets, the released moisture from the heated fuel may condense and be absorbed by the cold layers of the fuel, leading to expansion of the pellet grains and a further increase in the particle filtration efficiency.

However, during self-heating in a storage silo, the temperatures will increase at a much slower rate than in the experiments described here. It is therefore conceivable that during the significantly longer periods involved, LVOC-rich particles may both form and reach the top of the stored material. The particle concentration during the experiments reported in this work, increased by two orders of magnitude when the temperature increased only up to 100–110 °C. Under a much slower, spontaneous temperature increase in a large storage silo, particle concentrations at detectable levels may be established above the stored material.

Furthermore, in the tube oven experiments, air or nitrogen was pushed at 0.3 l/min for a 0.1 kg sample (with flow through the sample), while in the combustion chamber experiment air was pulled at 0.23 l/min for a 1 kg sample (with air extracted from the surroundings of the sample). It is conceivable that the air flow (outside and inside the sample) in the latter type of experiment was not high enough to suppress filtration by the unheated fuel material.

We expect low grain-to-grain variations in composition as well as low local variations in packing structure (from differences in grain size and details of the filling process) for the type of measurements reported here. This assumption is based on other experiments and measurements (to be reported elsewhere).

5. Conclusions

This study shows that heated wood pellets release low-volatility species and that at temperatures of above 85–90 °C (and most notably above 100 °C) these species lead to formation of sub-micron organic aerosols. This is observed under oxygen-free and oxygen-containing atmosphere. Our results show that in the lack of oxygen, CO and CO_2 are not reliable markers for the preheating and drying stages that precede pyrolysis and smoldering combustion. We suggest that the onset of high concentration of sub-micron particles may serve as a reliable marker for these stages. In the presence of oxygen, sub-micron particles are detected at a temperature that is 20–30 °C lower than what is required for significant and detectable changes in CO or CO_2 levels.

Furthermore, our results suggest that the existence of detectable CO levels depends on the presence of oxygen in ambient concentration that is preferably avoided in storage silos in order to reduce the risk of ignition.

In the experiments of the type shown in Fig. 2 no increase in particle concentration was detected, probably due to effective filtration by unheated pellets providing a relatively cold surface for condensation of fine mode particulate matter. For these reasons, the use of fine mode particles for early detection of smoldering fire could be challenging.

Thus, the new detection principle reported here cannot be implemented at industrial scale yet. A series of experiments, where both sample size, temperature distribution, air-flow rate through the sample, and duration are varied in a systematic way, will be necessary to determine if particle concentration may be used as a precursor of smoldering in large storage units.

CRediT authorship contribution statement

Nir Bluvshtein: Methodology, Investigation, Writing - original draft, Writing - review & editing. **Edmundo Villacorta:** Methodology, Investigation, Writing - review & editing. **Chunlin Li:** Methodology, Investigation, Writing - review & editing. **Bjarne C. Hagen:** Conceptualization, Writing - review & editing, Supervision, Funding acquisition.

Vidar Frette: Conceptualization, Writing - review & editing, Supervision, Project administration, Funding acquisition. **Yinon Rudich:** Conceptualization, Writing - review & editing, Supervision, Project administration.

Acknowledgements

This research was supported by The Research Council of Norway, project 238329: Emerging Risks from Smoldering Fires (EMRIS-collaboration) – and was partially supported by research grants from the US–Israel Binational Science Foundation (BSF Grant No. 2016093). C.L. acknowledges support from the Planning & Budgeting Committee, Israel (2018/19).

References

[1] Krause, U., Introduction, in *Fires in Silos*. 2009, Wiley-VCH Verlag GmbH & Co. KGaA. p. 1-11.
[2] K.K. Pant, P. Mohanty, Biomass, conversion routes and products – an overview, in: s Transformation of Biomas, John Wiley & Sons, Ltd., 2014, pp. 1–30.
[3] M. Considine, SELF-HEATING - evaluating and controlling the hazards - bowes,PC, Chemical Engineer-London (407) (1984), 68-68.
[4] D. Westermann, Fire in a silo for wood pellets in Esbjerg, Denmark, 1998-1999, in: U. Krause (Ed.), Fires in Silos: Hazards, Prevention, and Fire Fighting, WILEY-VCH Verlag GmbH & CO, Weinheim, 2009, pp. 93–110.
[5] D. Botnen, Rapport, Hallingdal Trepellets 5. Juli 2010, 2010.
[6] R.A. Ogle, S.E. Dillon, M. Fecke, Explosion from a smoldering silo fire, Process Saf. Prog. 33 (1) (2014) 94–103.
[7] P. Russo, A. De Rosa, M. Mazzaro, Silo explosion from smoldering combustion: a case study, Can. J. Chem. Eng. 95 (9) (2017) 1721–1729.
[8] R.P. Schifiliti, R.L.P. Custer, B. Meacham, Design of detection systems, in: M. J. Hurley (Ed.), SFPE Handbook of Fire Protection Engineering, Springer, New York, 2016, pp. 1314–1377.
[9] T. Chaudhry, K. Moinuddin, Method of identifying burning material from its smoke using attenuation of light, Fire Saf. J. 93 (2017) 84–97.
[10] P. Kanakam, S.M. Hussain, A.S.N. Chakravarthy, Electronic noses: forestalling fire disasters: a technique to prevent false fire alarms and fatal casualties, in: IEEE International Conference on Computational Intelligence and Computing Research (ICCIC), 2015, 2015.
[11] D. Madsen, et al., Levoglucosan as a tracer for smouldering fire, Fire Technol. 54 (6) (2018) 1871–1885.
[12] T.J. Ohlemiller, Modeling of smoldering combustion propagation, Prog. Energy Combust. Sci. 11 (4) (1985) 277–310.
[13] J.L. Torero, A.C. Fernandez-Pello, Natural convection smolder of polyurethane foam, upward propagation, Fire Saf. J. 24 (1) (1995) 35–52.
[14] A.V. Bridgwater, et al., The nature and control of solid, liquid and gaseous emissions from the thermochemical processing of biomass, Biomass Bioenergy 9 (1) (1995) 325–341.
[15] A.C. Aiken, P.F. DeCarlo, J.L. Jimenez, Elemental analysis of organic species with electron ionization high-resolution mass spectrometry, Anal. Chem. 79 (21) (2007) 8350–8358.
[16] D. Madsen, et al., Emerging risks from smouldering fires: initial results from the EMRIS project, in: INTERFLAM 2016, 2016. London.
[17] R.F. Mikalsen, et al., Extinguishing smoldering fires in wood pellets with water cooling: an experimental study, Fire Technol. 55 (2019) 257.
[18] R.F. Mikalsen, B.C. Hagen, V. Frette, Synchronized smoldering combustion, EPL (Europhysics Letters) 121 (5) (2018) 50002.
[19] A.C. Aiken, et al., O/C and OM/OC ratios of primary, secondary, and ambient organic aerosols with high-resolution time-of-flight aerosol mass spectrometry, Environ. Sci. Technol. 42 (12) (2008) 4478–4485.
[20] Q. Zhang, et al., Hydrocarbon-like and oxygenated organic aerosols in Pittsburgh: insights into sources and processes of organic aerosols, Atmos. Chem. Phys. 5 (12) (2005) 3289–3311.
[21] M.J. Cubison, et al., Effects of aging on organic aerosol from open biomass burning smoke in aircraft and laboratory studies, Atmos. Chem. Phys. 11 (23) (2011) 12049–12064.
[22] N.L. Ng, et al., Organic aerosol components observed in northern hemispheric datasets from aerosol mass spectrometry, Atmos. Chem. Phys. 10 (10) (2010) 4625–4641.
[23] R. Samuelsson, C. Nilsson, J. Burvall, Sampling and GC-MS as a method for analysis of volatile organic compounds (VOC) emitted during oven drying of biomass materials, Biomass Bioenergy 30 (11) (2006) 923–928.
[24] C.D. O'Dowd, et al., Atmospheric particles from organic vapours, Nature 416 (2002) 497.
[25] N. Fernandez Añez, et al., Detection of incipient self-ignition process in solid fuels through gas emissions methodology, J. Loss Prev. Process. Ind. 36 (2015) 343–351.
[26] A. Bougiatioti, et al., Processing of biomass-burning aerosol in the eastern Mediterranean during summertime, Atmos. Chem. Phys. 14 (9) (2014) 4793–4807.
[27] R.A. Washenfelder, et al., Biomass burning dominates brown carbon absorption in the rural southeastern United States, Geophys. Res. Lett. 42 (2) (2015) 653–664.
[28] J.L. Jimenez, et al., Evolution of organic aerosols in the atmosphere, Science 326 (5959) (2009) 1525–1529.
[29] S. Weimer, et al., Organic aerosol mass spectral signatures from wood-burning emissions: influence of burning conditions and wood type, J. Geophys. Res.: Atmosphere 113 (D10) (2008) n/a-n/a.
[30] Garcia-Perez, M., The Formation of Polyaromatic Hydrocarbons and Dioxins during Pyrolysis: A Review of the Literature With Descriptions of Biomass Composition, Fast Pyrolysis Technologies and Thermochemical Reactions 2008, Washington State University.